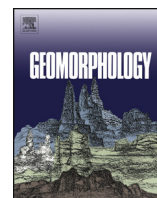




Contents lists available at ScienceDirect

Geomorphology

journal homepage: www.elsevier.com/locate/geomorph

Scaling and design of landslide and debris-flow experiments

Richard M. Iverson*

U.S. Geological Survey, 1300 SE Cardinal Ct., Vancouver, WA USA

ARTICLE INFO

Article history:

Received 24 July 2014

Received in revised form 20 February 2015

Accepted 23 February 2015

Available online xxx

Keywords:

Landslide

Debris flow

Experiment

Scaling

Dimensional analysis

Normalization

ABSTRACT

Scaling plays a crucial role in designing experiments aimed at understanding the behavior of landslides, debris flows, and other geomorphic phenomena involving grain-fluid mixtures. Scaling can be addressed by using dimensional analysis or – more rigorously – by normalizing differential equations that describe the evolving dynamics of the system. Both of these approaches show that, relative to full-scale natural events, miniaturized landslides and debris flows exhibit disproportionately large effects of viscous shear resistance and cohesion as well as disproportionately small effects of excess pore-fluid pressure that is generated by debris dilation or contraction. This behavioral divergence grows in proportion to H^3 , where H is the thickness of a moving mass. Therefore, to maximize geomorphological relevance, experiments with wet landslides and debris flows must be conducted at the largest feasible scales. Another important consideration is that, unlike stream flows, landslides and debris flows accelerate from statically balanced initial states. Thus, no characteristic macroscopic velocity exists to guide experiment scaling and design. On the other hand, macroscopic gravity-driven motion of landslides and debris flows evolves over a characteristic time scale $(L/g)^{1/2}$, where g is the magnitude of gravitational acceleration and L is the characteristic length of the moving mass. Grain-scale stress generation within the mass occurs on a shorter time scale, $H/(gL)^{1/2}$, which is inversely proportional to the depth-averaged material shear rate. A separation of these two time scales exists if the criterion $H/L < 1$ is satisfied, as is commonly the case. This time scale separation indicates that steady-state experiments can be used to study some details of landslide and debris-flow behavior but cannot be used to study macroscopic landslide or debris-flow dynamics.

Published by Elsevier B.V.

1. Introduction

Experimentation forms the backbone of most science, but it constitutes only a small fraction of the total body of work in geomorphology. Although controlled experiments provide a sure means of isolating the influences of key variables and performing definitive hypothesis tests, in geomorphology a question invariably arises about the relevance of experimental results. Critics commonly argue that experiments are too small, too brief, too idealized, or too restricted by artificial boundary or initial conditions to mimic the rich complexity of natural processes (e.g., Baker, 1996). To some extent these criticisms misconstrue the purpose of experimentation, which is not to imitate nature but instead to abstract it and thereby make it more amenable to systematic study (e.g., Gilbert, 1914). On the other hand, such criticisms can be valid if experiments misrepresent natural processes by abstracting them at inappropriate scales.

Scale plays a crucial role in many geomorphological experiments because it affects nearly all phenomena involving interaction of sediment and water. (One scale-dependent phenomenon is evident to anyone who builds a sandcastle. Forming damp sand into a free-standing vertical face 10 cm high is literally child's play, whereas forming a similar

face 10 m high is impossible.) Many scaling issues can be addressed by careful experiment design, however. This paper emphasizes scaling and experiment design as they apply to laboratory studies of subaerial mass movements such as landslides and debris flows, but the concepts it summarizes also have relevance in a broader geomorphological context.

2. Purposes of mass-movement experiments

Experimental studies of landslides and debris flows can target several broad classes of objectives, one of which is facilitation of field observations and measurements. Field experiments differ from laboratory experiments because they generally aim to retain the scale and complexity of natural processes while controlling their location and timing (Fig. 1). A common strategy involves instrumenting a natural hillside and watering it artificially until slope failure occurs (e.g., Ochiai et al., 2004, 2007; Springman et al., 2009). Similar watering experiments that do not lead to slope failure may transition into long-term field monitoring studies (e.g., Montgomery et al., 1997, 2009). Other field experiments bypass the onset of slope failure in order to focus on the dynamics of landslide or debris-flow runoff. These experiments typically involve controlled discharges of water or water – sediment mixtures onto instrumented natural slopes or channels (e.g., Rickenmann et al., 2003; Bugnion et al., 2012; Paik et al., 2012). Although field experiments

* Tel.: +1 360 993 8920; fax: +1 360 993 8980.
E-mail address: riverson@usgs.gov.



Fig. 1. Photograph of an instrumented natural hillside being prepared for a landslide-initiation experiment, Ibaraki prefecture, Japan, 2003 (see [Ochiai et al., 2004, 2007](#)). USGS photo by M.E. Reid.

can be large enough to avoid scaling problems, and complex enough to mimic nature, no field experiment is strictly reproducible because of the idiosyncrasies of the natural settings and materials involved.

Reproducible laboratory experiments differ fundamentally from field experiments because they are designed to idealize natural processes, minimize complexity, and thereby isolate the effects of key variables. These goals are attainable in a laboratory setting because initial conditions, boundary conditions, and material properties can

be closely controlled. Laboratories impose practical constraints on experiment scale, however. The largest laboratory mass-movement experiments to date have involved about 83 m^3 of material ([Moriwaki et al., 2004](#)) ([Fig. 2](#)), and many experiments have involved $<2 \text{ m}^3$ (e.g., [Eckersley, 1990](#); [Parsons et al., 2001](#); [Manzella and Labiouse, 2009](#)). Scaling is therefore a crucial – albeit sometimes overlooked – aspect of experiment design.

Scaling can be particularly challenging in laboratory experiments that aim not to test specific hypotheses but rather to strip away confounding influences that are prevalent in nature and thereby reveal phenomenology that is difficult to observe or measure in the field. Designs of such exploratory experiments can be very diverse (e.g., [Iverson et al., 2000](#); [Okura et al., 2000](#); [Bowman et al., 2012](#); [Hsu et al., 2014](#); [Kaitna et al., 2014](#); [Paguican et al., 2014](#)). Nevertheless, experiment design can be informed by using dimensional analysis to evaluate the potential scale-dependence of conspicuous physical phenomena, such as friction reduction by elevated pore-fluid pressure, and of less-conspicuous phenomena, such as apparent debris cohesion caused by electrostatic attraction of small particles or surface tension of air–water interfaces ([Iverson et al., 2004](#)).

Another class of laboratory experiments aims to test specific hypotheses that have been formalized in precise mathematical form ([Iverson, 2003a](#)). In these cases, normalization of a mathematical model's governing equations yields information about appropriate experiment scaling (e.g., [Iverson and Denlinger, 2001](#)). Experiments aimed at model testing are generally warranted only after the basic phenomenology of a process has been repeatedly observed and measured, however. A classic example of the progression from observations and measurements to systematic model development and testing is provided by the most famous scientific advances of the sixteenth and seventeenth centuries, when Galileo, Brahe, and Kepler established the empirical phenomenology that guided Newton's construction and testing of his mathematical theory of gravitation and rigid-body motion.

Physically based mathematical models of mass-movement processes apply the principles developed by Newton, but this application can be challenging because mass-movement models must account for the effects of energy dissipation. Indeed, dissipative processes produce most of the scale-dependent effects that can bedevil model formulation as well as systematic experimentation and data interpretation. For example, the energy expenditure necessary to overcome a debris yield strength of 0.1 kPa can be important in a miniaturized laboratory debris



Fig. 2. Photograph of the aftermath of a large-scale laboratory landslide experiment at the National Research Institute for Earth Science and Disaster Prevention (NEID), Tsukuba, Japan, 2003 (see [Moriwaki et al., 2004](#)). NEID photo by H. Moriwaki.

flow < 0.1 m thick (e.g., Parsons et al., 2001), but it is largely irrelevant in a full-scale debris flow > 1 m thick (Iverson, 2003b). Individual mass-movement experiments may therefore combine elements of the exploratory and model testing objectives described in the preceding paragraphs. In such experiments, scaling inferences derived from dimensional analysis can be merged with those derived from model normalization (e.g., Iverson et al., 2004, 2010). This paper considers dimensional analysis and model normalization as synergistic tools for experiment scaling and design.

3. Dimensional analysis

Dimensional analysis is founded on the principle of dimensional homogeneity, which has been understood since the birth of mathematical physics (Bolster et al., 2011). In simplest terms, dimensional homogeneity requires that the left-hand side of any physically valid equation must have dimensions like those of the right-hand side. To fully exploit this principle, Edgar Buckingham (1914, 1915) devised formalized methods of dimensional analysis that are still used today. These methods were elaborated by Percy Bridgman, a renowned experimentalist and Nobelist who remarked that dimensional analysis was quite foolproof when applied by someone with suitable experience and judgment, but that ‘the untutored [geomorphologist] in the bushes would probably not be able to apply the methods of dimensional analysis... and obtain results which would satisfy us’ (Bridgman, 1922, p. 5). In the foregoing quote, ‘geomorphologist’ facetiously replaces a pejorative term used by Bridgman, but in fact, all geomorphologists – even those of us who sometimes work among the bushes – have the skills necessary to obtain useful results by applying dimensional analysis. These results help prevent oversights in experiment design and also inform analysis of field observations and data.

A key concept introduced by Buckingham (1914, 1915) and embraced by Bridgman (1922) involved systematic identification of dimensionless variables known as Π groups. This name derives from Buckingham’s Π theorem, which states that any physically valid relationship between n_1 variables involving n_2 fundamental physical dimensions (for example, mass, length, and time) can be reduced to a relationship among $n_1 - n_2$ dimensionless variables. Expressing physical relationships in terms of dimensionless variables has deep theoretical significance because nature operates independently of human inventions, including our definitions of mass, length, and time. Therefore, any valid physical principle can be expressed in a dimensionless mathematical form that does not depend on such definitions.

Dimensionless Π groups also have great practical relevance for experiment design because they serve as scaling parameters that guide strategies for upsizing, downsizing, or simplifying an experiment. By isolating the effects of $n_1 - n_2$ dimensionless Π groups rather than those of n_1 dimensional variables, researchers can narrow the objectives of their experiments. Moreover, by holding the values of Π groups constant as an experiment is downsized relative to a natural phenomenon, an experimenter can create a valid scale model of a natural prototype.

3.1. Macroscopic dimensional analysis: blockslide or avalanche with no fluid

As an illustration of dimensional analysis applied to mass-movement experiments, first consider a rudimentary, macroscopic analysis of an infinitely wide mass of homogenous material that retains its macroscopic shape as it travels down a uniform slope in a vacuum (Fig. 3). This simplistic view of a landslide omits any consideration of a fluid phase (either air or water), but it provides a useful starting point. The goal of the analysis is to draw inferences about dimensionless variables that control the evolving downslope velocity \bar{u} of the moving mass. The fact that \bar{u} evolves during the course of a mass movement is fundamental because, unlike some other geomorphological phenomena,

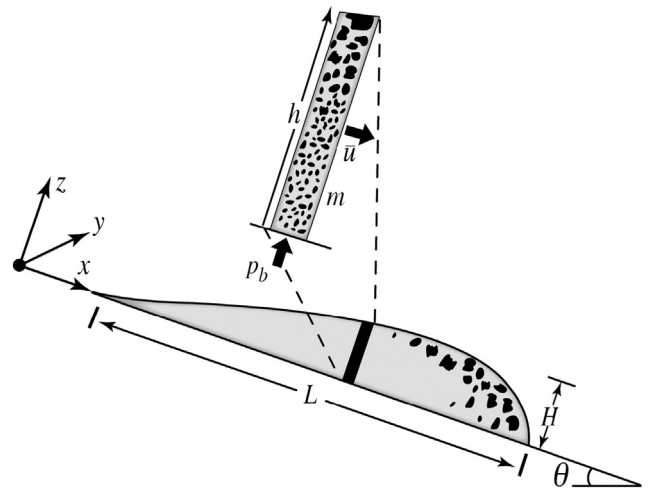


Fig. 3. Schematic vertical cross section of a moving mass descending a plane inclined at the angle θ . The thickness and length of the mass are H and L , respectively. One slice of the mass is magnified to depict key dependent variables considered in analyses. In the simplest analysis (section 3.1), only the depth-averaged downslope velocity \bar{u} evolves with time. In more sophisticated analyses (Sections 3.2 and 4), H and L also evolve, as do the local thickness h , basal pore-fluid pressure, p_b , and solid volume fraction, m (which affects the debris bulk density, ρ) (after Iverson and George, 2014).

most mass-movement processes are inherently unsteady. They lack a characteristic velocity, and they have distinct starting and ending points in space and time.

The first step in the analysis consists of using physical intuition and the sketch in Fig. 3 to make a list of macroscopic variables that might influence evolution of \bar{u} . A basic list includes the moving mass’s bulk density, ρ , length, L , and thickness, H , as well as the acceleration due to gravity, g , slope angle, θ , time, t , and basal Coulomb friction angle, ϕ . In this simple approach, ϕ parameterizes the effects of energy dissipation during basal sliding, and any effects of internal deformation on energy dissipation are subsumed within a generic stress variable, σ . The postulated effects of this list of variables can then be summarized as

$$\bar{u} = f_1(g, L, H, \rho, \sigma, \theta, \phi, t) \quad (1)$$

where f_1 represents an unknown function.

Eq. (1) includes two intrinsically dimensionless variables (θ and ϕ) as well as seven dimensional variables (\bar{u} , g , L , H , ρ , σ , and t). Variables that are intrinsically dimensionless play no role in identification of new dimensionless variables, indicating that θ and ϕ can be temporarily ignored. The remaining seven variables in Eq. (1) involve various combinations of three fundamental physical dimensions: mass, length, and time. Therefore, Buckingham’s Π theorem indicates that these seven dimensional variables must be related in a manner that can be expressed by $7 - 3 = 4$ independent dimensionless variables. To identify these four variables, the functional relation in Eq. (1) is first postulated to have the generic form

$$\bar{u} = \kappa g^a L^b H^c \rho^d \sigma^e t^f \quad (2)$$

in which values of a , b , c , d , e , and f are unknown and κ is a dimensionless proportionality factor. By expressing all physical variables in Eq. (2) in terms of their dimensions, which involve various combinations of mass [M], length [L], and time [T], Eq. (2) can be recast as

$$\frac{[L]}{[T]} = \left(\frac{[L]}{[T]^2}\right)^a [L]^b [L]^c \left(\frac{[M]}{[L]^3}\right)^d \left(\frac{[M]}{[L][T]^2}\right)^e [T]^f \quad (3)$$

This equation is dimensionally homogeneous (and physically plausible) only if powers of [M], [L], and [T] are the same on its left-hand and right-

hand sides. Equating these powers yields three conditions that must be satisfied:

- condition for homogeneity of [M]: $0 = d + e$,
- condition for homogeneity of [L]: $1 = a + b + c - 3d - e$, and
- condition for homogeneity of [T]: $-1 = -2a - 2e + f$.

These conditions constitute three simultaneous algebraic equations containing six unknowns (a, b, c, d, e , and f), implying that three of the unknowns can be eliminated. For example, a, b , and d can be eliminated algebraically by finding that $a = (1/2) - e + (f/2)$, $b = (1/2) - c - e - (f/2)$, and $d = -e$. Use of these substitutions in Eq. (2) then yields

$$\bar{u} = \kappa g^{(1/2)-e+(f/2)} L^{(1/2)-c-e-(f/2)} H^c \rho^{-e} \sigma^e t^f \quad (4)$$

and grouping terms that share the same exponents reduces Eq. (4) to

$$\bar{u} = \kappa (gL)^{1/2} \left(\frac{H}{L}\right)^c \left(\frac{\sigma}{\rho g L}\right)^e \left(\frac{t}{(L/g)^{1/2}}\right)^f \quad (5)$$

By dividing each side of Eq. (5) by $(gL)^{1/2}$ and reintroducing the intrinsically dimensionless variables θ and ϕ , the general functional relationship postulated in Eq. (1) can be recast in the dimensionless form,

$$\frac{\bar{u}}{(gL)^{1/2}} = f_2 \left(\frac{H}{L}, \frac{\sigma}{\rho g L}, \frac{t}{(L/g)^{1/2}}, \theta, \phi \right) \quad (6)$$

where f_2 represents a new unknown function. As anticipated from Buckingham's Π theorem, Eq. (6) contains only six dimensionless variables rather than the original nine variables contained in Eq. (1). Note that L serves as the fundamental length scale in Eq. (6) because it appears in the denominator of every variable except θ and ϕ . Moreover, $(L/g)^{1/2}$ serves as the fundamental time scale over which \bar{u} evolves.

Eq. (6) is entirely valid but is not unique. If c rather than b had been selected for elimination in the algebraic step leading to Eq. (4), for example, then H and L would trade positions in Eq. (6), and H would serve as the fundamental length scale. This nonuniqueness indicates that it is justifiable to revise the Π groups in Eq. (6) by combining existing groups via multiplications or divisions – particularly if such algebraic manipulation is motivated by physical experience and insight. In the case of Eq. (6), experience with the effects of gravity on rock and soil makes it logical to expect that stress will scale with the thickness H rather than the length L of a mass. Therefore, it is reasonable to divide $\sigma/\rho g L$ by H/L in Eq. (6) and thereby obtain the revised Π group, $\sigma/\rho g H$. This modification yields a relationship among dimensionless variables that is suitable for guiding experiment design:

$$\frac{\bar{u}}{(gL)^{1/2}} = f_3 \left(\frac{H}{L}, \frac{\sigma}{\rho g H}, \frac{t}{(L/g)^{1/2}}, \theta, \phi \right) \quad (7)$$

A trivial experiment that could be designed with the aid of Eq. (7) involves motion of a rigid block with constant H, L, ρ , and σ descending an inclined plane. Even for this simple experiment, however, Eq. (7) provides useful guidance because it indicates that \bar{u} scales with $(gL)^{1/2}$ while t scales with $(L/g)^{1/2}$. Taken together, these scalings imply that \bar{u} is proportional to gt , and Eq. (7) further implies that the proportionality will depend on the values of θ and ϕ . These findings predict the ingredients of the exact equation describing motion of a sliding block released from a state of rest at $t = 0$ (i.e., $\bar{u} = gt(\sin \theta - \cos \theta \tan \phi)$). If this equation were unknown, then dimensional analysis would facilitate its discovery through experimentation using a single block and several inclined planes with various combinations of θ and ϕ . Furthermore, no

information in Eq. (7) suggests that the effects of θ and ϕ on \bar{u}/gt would be influenced by the size of the experimental apparatus. Therefore, a researcher could reasonably infer that results of miniaturized experiments with rigid sliding blocks might apply to analogous sliding blocks at large scales. Few if any natural landslides behave as rigid blocks, however.

A more relevant type of mass-movement experiment involves motion of a deformable avalanche consisting of millions of dry, rigid grains (Fig. 4). In this case Eq. (7) still applies, but none of the quantities in Eq. (7) can be viewed as constants. The inference $\bar{u} \propto gt$ remains the same as for a rigid sliding block, but in a deforming avalanche \bar{u} varies from point to point as H/L evolves. Concurrently, $\sigma/\rho g H$ may evolve for a variety of reasons: ρ may change as a result of dilation or contraction of the granular material, vertical acceleration components may modify the effective g force on avalanching grains, or granular momentum exchange might transition from a contact-dominated to collision-dominated mode. In any case, an experiment designed to track evolution of the most easily measured stress component, the basal normal stress, would help constrain evolution of $\sigma/\rho g H$ with time and position along the avalanche path. Spatially distributed measurements of the evolving basal normal stress could then be combined with measurements of H/L and $\bar{u}/(gL)^{1/2}$ in an effort to uncover the factors controlling avalanche dynamics along paths with differing values of θ and ϕ .

A caveat in such granular avalanche experiments is that scale effects might be important. A likely cause is scale-dependence of the relatively poorly characterized processes that influence $\sigma/\rho g H$. Thus, while many useful bench-top experiments with dry granular avalanches have been conducted during the past few decades (e.g., Densmore et al., 1997; Iverson et al., 2004; Pudasaini and Hutter, 2007; Mangeney et al., 2010), their geomorphological relevance should perhaps be taken with a grain of salt. Indeed, the presumption that large, natural landslides ought to behave like miniature avalanches of dry granular material led to a longstanding misperception in landslide science. Beginning with Heim (1882), as recapitulated by Hsü (1978), many investigators once regarded the mobility of large landslides as anomalous if the ratio of horizontal runout distance to vertical descent distance exceeded about 1.7, a value that is typical of laboratory-scale sand avalanches (Dade and Huppert, 1998). These miniature avalanches omit a number of scale-dependent phenomena that can influence the behavior of large landslides, however. One of the most obvious scale dependencies involves modification of $\sigma/\rho g H$ by pore-fluid pressure (Legros, 2002).

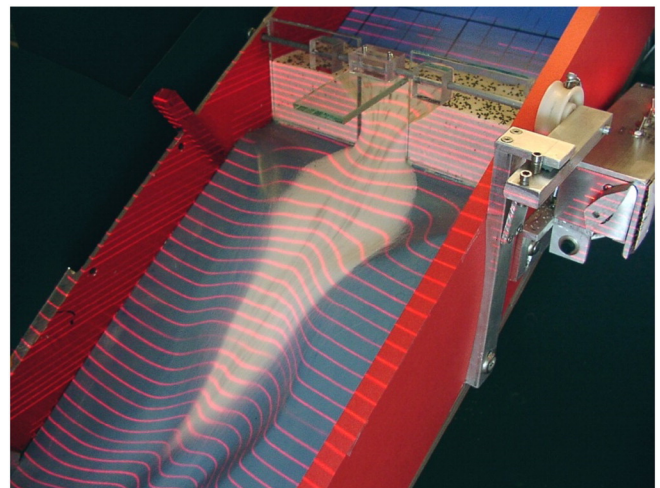


Fig. 4. Photograph of a small-scale experiment involving an avalanche of dry sand in a flume 20 cm wide. Avalanche motion is instigated by sudden opening of a headgate. Topographic contours (red lines) are projected onto the flume bed (blue) and the sand surface (white) by horizontal laser sheets (see Iverson et al., 2004). USGS photo by M. Logan.

3.2. Macroscopic dimensional analysis: fluid-filled landslide or debris flow

Fluid plays a vital role in all debris flows and in many other landslides, and incorporation of fluid effects in experiments can increase their geomorphological relevance. However, the presence of fluid also complicates dimensional analysis, experiment scaling, and data interpretation. In general the ambient fluid adjacent to a mass as well as the intergranular fluid within a mass might be important, but the dimensional analysis presented here considers only the effects of intergranular pore fluid. This simplification is warranted for many dense, subaerial mass movements because the surrounding air exerts negligible buoyancy or inertial reaction forces.

Physical properties of an intergranular pore fluid include its density, ρ_f , viscosity, μ_f , elastic bulk modulus (reciprocal compressibility), E_f , and possibly its yield strength, c_f – a property that may be relevant if the fluid contains suspended mud (Table 1). Properties of solid grains, which are treated here as incompressible, include their density, ρ_s , and friction angle, ϕ . The solid volume fraction m (and the porosity, $1 - m$) can evolve in a deforming debris flow or landslide so that the compressibility of the bulk solid-fluid mixture – or its reciprocal, the mixture bulk modulus, E – can be important (Iverson and George, 2014). If the value of m is known and those of ρ_s and ρ_f are also known, then the evolving mixture bulk density ρ need not be considered independently because $\rho = \rho_s m + \rho_f(1 - m)$ must be satisfied. Nevertheless, it is useful to define a fixed reference value of ρ that

applies in an undeformed initial state. Here ρ_0 denotes this reference value, which applies when $m = m_0$. Another important bulk property is the Darcian pore-fluid permeability k of the granular solid aggregate. In general the value of k evolves as that of m evolves (Iverson and George, 2014), but here the analysis considers only a representative, fixed value of k that summarizes the Darcian permeability of a mixture of grains with diverse shapes and sizes (Table 1). Addition of these material properties to the list of variables considered in Eq. (1) yields an expanded functional relation:

$$\bar{u} = f_4(g, L, H, \rho_0, \rho_s, \rho_f, \sigma, \theta, \phi, \mu_f, c_f, E_f, E, k, m, t) \tag{8}$$

According to Buckingham's Π theorem, Eq. (8) can be reduced from a relation involving 17 variables to one involving 14 dimensionless Π groups. In these Π groups it is desirable to retain the fundamental time scale $(L/g)^{1/2}$, velocity scale $(Lg)^{1/2}$, and mass scale $\rho_0 H^3$ inferred from Eq. (7). Indeed, identification of fundamental scales is a compelling reason to perform a simple dimensional analysis like that in section 3.1 before undertaking dimensional analysis of a relationship as lengthy as Eq. (8). Otherwise, the best choice of fundamental scales may not be obvious. This choice guides the selection of algebraic cancellations, multiplications, and divisions that are necessary to obtain the most useful set of Π groups.

By using a mathematical procedure exactly analogous to that used to obtain Eq. (7), while retaining the fundamental scales $(L/g)^{1/2}$, $(Lg)^{1/2}$,

Table 1

Summary of all variables used in all dimensional analyses and in equation normalization (excluding those dimensionless variables defined and denoted by asterisks in Eq. (15)).

Symbol	Definition	Dimensions	SI Units
c_f	cohesive shear strength of fluid phase containing mud	$[M][L]^{-1}[T]^{-2}$	Pa
D	depth-integrated debris dilation rate	$[L][T]^{-1}$	$m \cdot s^{-1}$
e_s	coefficient of restitution of solid grains	0	--
E	elastic bulk modulus of solid-fluid mixture	$[M][L]^{-1}[T]^{-2}$	Pa
E_f	elastic bulk modulus of fluid phase	$[M][L]^{-1}[T]^{-2}$	Pa
E_s	elastic bulk modulus of solid grains	$[M][L]^{-1}[T]^{-2}$	Pa
g	magnitude of gravitational acceleration	$[L][T]^{-2}$	$m \cdot s^{-2}$
g_i	i -direction component of gravitational acceleration	$[L][T]^{-2}$	$m \cdot s^{-2}$
h	local thickness of moving mass	[L]	m
H	characteristic thickness of moving mass	[L]	m
k	Darcian hydraulic permeability of granular mass	$[L]^2$	m^2
L	characteristic length of moving mass	[L]	m
m	solid volume fraction of granular mass	0	--
m_0	characteristic (initial) value of m	0	--
m_{crit}	static, critical-state value of m	0	--
N	dimensionless state parameter	0	--
p_b	basal pore-fluid pressure	$[M][L]^{-1}[T]^{-2}$	Pa
t	time coordinate	[T]	s
\bar{u}	depth-averaged mixture velocity in x direction	$[L][T]^{-1}$	$m \cdot s^{-1}$
\bar{v}	depth-averaged mixture velocity in y direction	$[L][T]^{-1}$	$m \cdot s^{-1}$
\bar{w}	depth-averaged mixture velocity in z direction	$[L][T]^{-1}$	$m \cdot s^{-1}$
x, y, z	position coordinates	[L]	m
Γ_f	surface tension of fluid phase	$[M][T]^{-2}$	$N \cdot m^{-1}$
$\dot{\gamma}$	debris shear rate	$[T]^{-1}$	s^{-1}
δ_s	modal diameter of solid grains	[L]	m
ε	$= H/L$	0	--
ζ_s	measure of dispersion of grain diameters	0	--
ϕ	friction angle of granular mass	0	--
θ	slope angle of substrate	0	--
κ	proportionality coefficient	0	--
λ_x	measure of sphericity of grains	0	--
ξ_s	measure of angularity of grains	0	--
μ_f	viscosity of fluid phase	$[M][L]^{-1}[T]^{-1}$	$Pa \cdot s$
ρ_f	mass density of fluid phase	$[M][L]^{-3}$	$kg \cdot m^{-3}$
ρ_s	mass density of solid grains	$[M][L]^{-3}$	$kg \cdot m^{-3}$
ρ_0	characteristic mass density of solid-fluid mixture	$[M][L]^{-3}$	$kg \cdot m^{-3}$
σ	stress component (generic)	$[M][L]^{-1}[T]^{-2}$	Pa
τ_{ii}	normal-stress component, $i = x, y, \text{ or } z$	$[M][L]^{-1}[T]^{-2}$	Pa
τ_{ij}	shear-stress component, $i, j = x, y, \text{ or } z$ ($i \neq j$)	$[M][L]^{-1}[T]^{-2}$	Pa
$\langle u^2 \rangle^{1/2}, \langle \omega^2 \rangle^{1/2}$	root mean square translational and rotational grain velocities	$[L][T]^{-1}$	$m \cdot s^{-1}$

and $\rho_0 H^3$, Eq. (8) can be reduced to a functional relationship involving 14 Π groups:

$$\frac{\bar{u}}{(gL)^{1/2}} = f_s \left(\frac{H}{L}, \frac{\sigma}{\rho_0 g H}, \frac{t}{(L/g)^{1/2}}, \theta, \phi, m, \frac{\rho_s}{\rho_0}, \frac{\rho_f}{\rho_0}, \frac{c_f}{\rho_0 g H}, \frac{E_f}{\rho_0 g H}, \frac{E}{\rho_0 g H}, \frac{(L/g)^{1/2}}{\mu_f H^2 / k E}, \frac{\rho_0 H (gL)^{1/2}}{\mu_f} \right) \quad (9)$$

The first six dimensionless variables in Eq. (9) are the same as those in Eq. (7). The next six variables in Eq. (9) have straightforward physical interpretations. They consist of the solid volume fraction, m , simple density ratios, ρ_s/ρ_0 and ρ_f/ρ_0 , a scaled yield strength, $c_f/\rho_0 g H$, and scaled bulk moduli, $E_f/\rho_0 g H$ and $E/\rho_0 g H$. Typical values of E_f for water and air at Earth's surface are about 2.2×10^9 Pa and 1×10^5 Pa, respectively, implying that $E_f/\rho_0 g H \gg 1$ is satisfied for mass movements of virtually any size if they contain water, whereas $E_f/\rho_0 g H \gg 1$ is satisfied for mass movements containing air only if H is smaller than about 1 m. Therefore, it is reasonable to infer that compressional deformation of water plays a minimal role in mass movements of all sizes, but that compression of air within very large mass movements could produce important effects that are less pronounced at laboratory scales (cf. Shreve, 1968; Roche et al., 2010). Finally, the Π group $c_f/\rho_0 g H$ in Eq. (9) implies that the effects of c_f can be exaggerated in miniaturized experiments that have H values much smaller than those of large landslides or debris flows (Iverson, 2003b).

From the standpoint of experiment scaling, the final two dimensionless variables in Eq. (9) are of greatest interest, and each involves the fluid viscosity, μ_f . The first of these variables can be interpreted as a time scale ratio because the numerator $(L/g)^{1/2}$ is the time scale for gravity-driven downslope motion of a landslide or debris flow, and the denominator $\mu_f H^2 / k E$ is the time scale for slope-normal diffusion of excess pore-fluid pressure that is generated by porosity changes. Recognition of this time scale requires some prior familiarity with well-established pore-pressure diffusion theory (e.g., Rice and Cleary, 1976), because pore pressure itself is not explicitly included in Eq. (9). Instead, pore pressure is subsumed within the normalized generic stress variable, $\sigma/\rho_0 g H$. Nevertheless, the presence in Eq. (9) of a Π group containing the pore-pressure diffusion time scale $\mu_f H^2 / k E$ is unsurprising because the dynamics of landslides and debris flows are commonly regulated by pore-pressure diffusion coupled to internal deformation (Iverson, 2005; Schaeffer and Iverson, 2008; George and Iverson, 2014). The final Π group in Eq. (9) is also easy to interpret because $\rho_0 H (gL)^{1/2} / \mu_f$ constitutes a Reynolds number in which $(gL)^{1/2}$ serves as

a velocity scale. This Reynolds number summarizes the ratio of bulk inertial forces to viscous shear resistance in a fluid-filled, gravity-driven moving mass that has a finite length L but no characteristic velocity.

The Π groups $(L/g)^{1/2} / (\mu_f H^2 / k E)$ and $\rho_0 H (gL)^{1/2} / \mu_f$ have a crucial ramification for experiment design because $\mu_f H^2$ appears in the denominator of one of them, while μ_f / H appears in the denominator of the other if it is rewritten as $\rho_0 (gL)^{1/2} / (\mu_f / H)$. Thus, if μ_f is held constant while H is reduced (i.e., from field scale to laboratory scale), then the importance of viscous shear resistance becomes disproportionately large while that of pore-pressure diffusion becomes disproportionately small (Fig. 5). Manipulating the value of μ_f in experiments cannot alleviate this scaling problem because modification of μ_f alters the values of $(L/g)^{1/2} / (\mu_f H^2 / k E)$ and $\rho_0 H (gL)^{1/2} / \mu_f$ proportionately.

A seemingly plausible but ultimately futile strategy for addressing the scaling problem noted above might involve holding the ratio of the parameters $(L/g)^{1/2} / (\mu_f H^2 / k E)$ and $\rho_0 H (gL)^{1/2} / \mu_f$ constant, while H is reduced from field scale to laboratory scale. The resulting ratio, $kE/\rho_0 g H^3$, constitutes a viable Π group. Evaluation of this Π group for a dense, flowing body of water-saturated sand and gravel with $H = 1$ m, $k \sim 10^{-9} \text{ m}^2$ and $E \sim 10^6$ Pa yields $kE/\rho_0 g H^3 \sim 10^{-6}$. Evaluation of the same Π group for a miniaturized body of water-saturated fine sand with $H = 0.02$ m, $k \sim 10^{-12} \text{ m}^2$, and $E \sim 10^5$ Pa also yields $kE/\rho_0 g H^3 \sim 10^{-6}$. Thus, the value of $kE/\rho_0 g H^3$ can be preserved by changing the material composition while downsizing H from 1 to 0.02 m. Scaling that considers $kE/\rho_0 g H^3$ and only one of the groups $(L/g)^{1/2} / (\mu_f H^2 / k E)$ or $\rho_0 H (gL)^{1/2} / \mu_f$ might therefore lead to the spurious inference that valid downsizing of experiments is feasible. This strategy does not address the conflicting effect that downsizing has on the values of $(L/g)^{1/2} / (\mu_f H^2 / k E)$ and $\rho_0 H (gL)^{1/2} / \mu_f$, however. Instead it illustrates a pitfall that can arise from injudicious selection of Π groups. In general a group such as $kE/\rho_0 g H^3$, which has an opaque physical meaning, is less useful than Π groups that have clear physical meanings.

To date no satisfactory strategy has been proposed for avoiding the scaling problem manifested in the Π groups $(L/g)^{1/2} / (\mu_f H^2 / k E)$ and $\rho_0 H (gL)^{1/2} / \mu_f$, and these Π groups have large implications for evaluating the effects of pore fluid in reducing effective basal friction. Experiments that artificially mimic the effects of such friction reduction have entailed installation of a viscous basal layer in miniature laboratory landslides (Paguican et al., 2014), but this mimicry does not constitute physical similitude. Thus, the most viable alternative for designing properly scaled experiments involving fluid-laden landslides and debris flows is to build

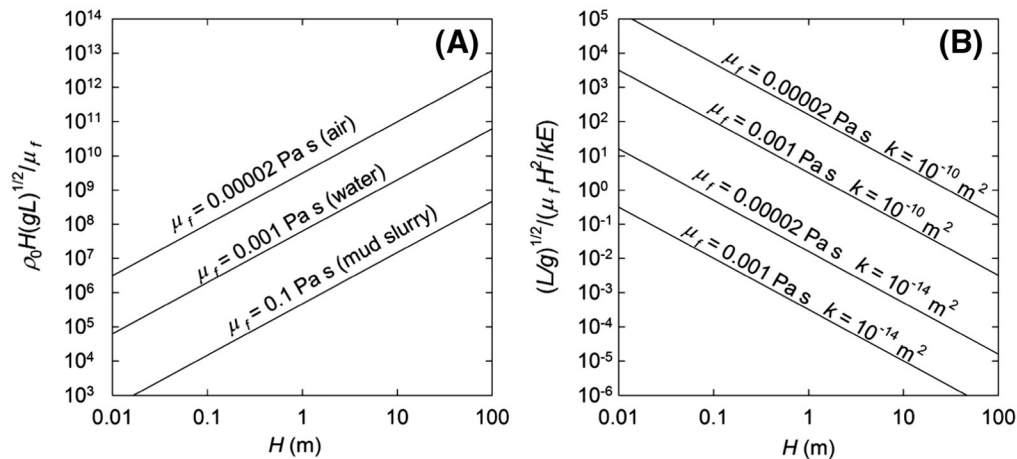


Fig. 5. Graphs of the Reynolds number $\rho_0 H (gL)^{1/2} / \mu_f$ and time scale ratio $(L/g)^{1/2} / (\mu_f H^2 / k E)$ as functions of landslide or debris-flow size (as measured by thickness H) for values of fluid viscosity typical of air ($\mu_f = 0.00002$ Pa s), water ($\mu_f = 0.001$ Pa s), and mud slurry ($\mu_f = 0.1$ Pa s); and for values of hydraulic permeability typical of clean sand ($k = 10^{-10} \text{ m}^2$) and poorly sorted debris with a muddy matrix ($k = 10^{-14} \text{ m}^2$). To generate these graphs, fixed values were assumed for three other quantities: the length-scale ratio $H/L = 100$ (typical of many mass movements), the compressive stiffness $E = 10^7$ Pa (typical of loose granular soils), and the bulk density $\rho_0 = 1500 \text{ kg/m}^3$ (typical of loosely packed granular soils). After Iverson et al. (2004).

and utilize the largest feasible laboratory facilities. This rationale prompted construction of the National Research Institute for Earth Science and Disaster Prevention (NIED) large-scale rainfall simulator and landslide test facility in Japan in 1974 (Fig. 2), and also prompted construction of the large-scale U.S. Geological Survey debris-flow flume in Oregon in 1991 (Figs. 6 and 7). Even at these facilities, however, experimental mass movements cannot duplicate all behavior that might occur in large natural events.

3.3. Mesoscopic dimensional analysis: steady shear flow of a solid–fluid mixture

A different style of experiment addresses the internal dynamics of grain – fluid mixtures without attempting to simulate the large-scale dynamics of mass movements or the small-scale dynamics of individual grains. These mesoscale experiments commonly focus on steady, uniform shear flows of nearly identical grains immersed in liquid (Fig. 8). By examining simple deformations of idealized materials, such experiments can reveal details of behavior that otherwise would be inaccessible (e.g., Bagnold, 1954; Iverson and LaHusen, 1989; Armanini et al., 2005; DeBoeuf et al., 2009; Boyer et al., 2011). Results of such experiments lack direct geomorphological relevance, but they can help build understanding of the more-complicated materials involved in geomorphic phenomena.

In steady-state experiments with idealized materials, stress is typically treated as a dependent variable while bulk flow velocity is controlled or at least well-constrained. By contrast, the macroscopic approach of Sections 3.1 and 3.2 treats stress as an independent variable, which influences the unconstrained bulk velocity of a landslide or debris flow. This difference in approaches is justified because stress is a continuum-scale quantity that summarizes the effects of momentum exchange processes operating at scales too small to be observed at the scale of a landslide or debris flow. Indeed, a chief objective of mesoscale experiments and dimensional analyses is to draw inferences about grain – grain and grain – fluid interactions that may influence stresses at larger scales.

Another distinction between macroscopic and mesoscopic dimensional analyses involves the role of time. The analyses in Sections 3.1 and 3.2 treat time as an independent variable, whereas the mesoscopic analysis presented here considers steady shear flows in which the



Fig. 7. Photograph of water application during a landslide initiation experiment involving a rectangular 6-m³ sediment prism positioned behind a retaining wall near the top of USGS debris-flow flume in Oregon, USA. Landslide onset was triggered by gradually rising pore-water pressure (see Iverson et al., 1997, 2000; Reid et al., 1997). Video recordings of this experiment and many similar experiments are viewable at <http://pubs.usgs.gov/of/2007/1315/> (see Logan and Iverson, 2007).

observable dynamics of the system are time-invariant. This distinction is warranted because landslide behavior commonly involves a separation of time scales. Large-scale landslide motion evolves over the macroscopic time scale $t_{macro} \sim (L/g)^{1/2}$, as noted in Sections 3.1 and 3.2, whereas mesoscopic grain interactions occur on a time scale given by the reciprocal of the shear rate (Goldhirsch, 2003). The

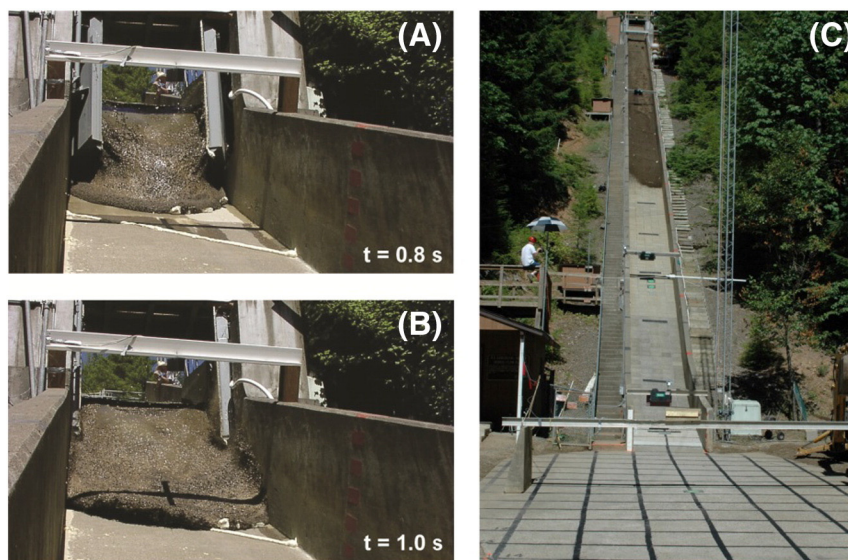


Fig. 6. Photographs of a large-scale experiment in which a 10-m³ debris flow was released from the headgate of the USGS debris-flow flume. Panels (A) and (B) show flow front at times 0.8 and 1.0 s after the headgate began to open. Panel (C) shows debris flow descending flume about 5 s after headgate began to open. Flume is 95 m long and 2 m wide. Most of the flume slopes uniformly at 31° (after Iverson et al., 2010). Video recordings of this experiment and many similar experiments are viewable at <http://pubs.usgs.gov/of/2007/1315/> (see Logan and Iverson, 2007).



Fig. 8. Close-up stop-action photograph of an idealized mass-movement experiment in which a water-submerged, close-packed array of cylindrical fiberglass rods (each with diameter 1.9 cm) moves steadily from right to left across the surface of a similar array, resulting in momentary hydroplaning caused by transient support of the moving array's entire weight by basal pore-fluid pressure. Device visible at top of image is a specially fabricated LED digital timer with resolution 0.01 s (see Iverson and LaHusen, 1989).

depth-averaged shear rate $\dot{\gamma}$ may be estimated as $\dot{\gamma} \sim \bar{u}/H$, and because \bar{u} scales with $(Lg)^{1/2}$, the time scale associated with the reciprocal shear rate may be estimated as $t_{meso} \sim H/(Lg)^{1/2}$. Thus, the ratio of the time scales for shear deformation and evolution of downslope landslide motion may be expressed as

$$\frac{t_{meso}}{t_{macro}} \sim \frac{H/(gL)^{1/2}}{(L/g)^{1/2}} = \frac{H}{L} \quad (10)$$

The timescale ratio therefore reduces to the geometric ratio H/L that appears in Eqs. (7) and (9). Because many landslides and debris flows have geometries that satisfy $H/L < 1$ (Fig. 3), separation of the time scales for internal shear deformation and evolution of macroscopic landslide or debris-flow motion is commonly justified.

Dimensional analyses of steady, uniform shear flows can build on a foundation established by Savage's (1984) analysis of dry granular flows. To have relevance for landslides and debris flows, however, Savage's (1984) analysis must be generalized to include the effects of intergranular fluid. Making this generalization, the mixture shear stress τ_{zx} and normal stress τ_{zz} on planes of shearing are postulated to be functions of 22 variables:

$$\tau_{zx}, \tau_{zz} = f_6 \left(\dot{\gamma}, \langle v^2 \rangle^{1/2}, \langle \omega^2 \rangle^{1/2}, H, g, m, \phi, k, \rho_s, \rho_f, E_s, E_f, \delta_s, \zeta_s, e_s, \lambda_s, \xi_s, \mu_f, \Gamma_f, c_f \right) \quad (11)$$

Variables in Eq. (11) that did not appear in Sections 3.1 and 3.2 are the one-dimensional mixture shear rate, $\dot{\gamma}$, the translational and rotational components of root-mean-square local grain velocities, $\langle v^2 \rangle^{1/2}$ and $\langle \omega^2 \rangle^{1/2}$, the fluid-phase surface tension, Γ_f , and a host of solid grain properties, including the elastic bulk modulus, E_s , coefficient of restitution, e_s , modal grain diameter, δ_s , dispersion of grain diameters, ζ_s , grain sphericity, λ_s , and grain angularity, ξ_s (Table 1). Even this extended list of variables is too brief to characterize the complexity of some natural grain-fluid mixtures, but it provides an indication of the range of complexities involved.

The choice of fundamental scales influences the outcome of a dimensional analysis of (11). The fundamental time scale is clearly given by the reciprocal of the shear rate, $1/\dot{\gamma}$, as noted above. One choice for the fundamental length scale is the modal grain diameter, δ_s , and the associated mass scale is then $\rho_s \delta_s^3$. These choices lead to a Bagnold stress scaling, wherein τ_{zx} and τ_{zz} each scale with $\rho_s \delta_s^2 \dot{\gamma}^2$ (cf. Bagnold, 1954; Hunt et al., 2002). Alternatively, if the fundamental length scale is chosen as H , then the associated scale for stresses is $\rho_s g H$. This gravitational

stress scaling may be a more appropriate choice for mass movements in which stress generation is dominated by enduring grain contacts rather than by the binary grain collisions considered by Bagnold (1954). Here, the implications of each of these scaling choices are considered in turn.

Adopting the Bagnold stress scaling and carrying out a dimensional analysis in the manner of section 3.1 reduces Eq. (11) to

$$\frac{\tau_{zx}}{\rho_s \delta_s^2 \dot{\gamma}^2}, \frac{\tau_{zz}}{\rho_s \delta_s^2 \dot{\gamma}^2} = f_7 \left(\frac{\langle v^2 \rangle^{1/2}}{\delta_s \dot{\gamma}}, \frac{\langle \omega^2 \rangle^{1/2}}{\delta_s \dot{\gamma}}, \frac{H}{\delta_s}, \frac{k}{\delta_s^2}, \frac{\rho_f}{\rho_s}, \frac{g}{\delta_s \dot{\gamma}^2}, \frac{E_s}{\rho_s \delta_s^2 \dot{\gamma}^2}, \frac{E_f}{\rho_s \delta_s^2 \dot{\gamma}^2}, \frac{\mu_f}{\rho_s \delta_s^2 \dot{\gamma}}, \frac{\Gamma_f}{\rho_s \delta_s^2 \dot{\gamma}^3}, \frac{c_f}{\rho_s \delta_s^2 \dot{\gamma}^2}, m, \phi, \zeta_s, e_s, \lambda_s, \xi_s \right) \quad (12)$$

This relationship involves 19 dimensionless Π groups and provides clear evidence that even simple experiments with complex granular mixtures can be difficult to design in way that will yield unambiguous conclusions about the mechanisms that generate stress. On the other hand, if experiments employ mixtures of identical rigid spheres fully immersed in an incompressible Newtonian liquid, then many of the variables in Eq. (12) are irrelevant, and the equation reduces to a significantly simpler form:

$$\frac{\tau_{zx}}{\rho_s \delta_s^2 \dot{\gamma}^2}, \frac{\tau_{zz}}{\rho_s \delta_s^2 \dot{\gamma}^2} = f_8 \left(\frac{\langle v^2 \rangle^{1/2}}{\delta_s \dot{\gamma}}, \frac{\langle \omega^2 \rangle^{1/2}}{\delta_s \dot{\gamma}}, \frac{H}{\delta_s}, \frac{k}{\delta_s^2}, \frac{\rho_f}{\rho_s}, \frac{g}{\delta_s \dot{\gamma}^2}, \frac{\mu_f}{\rho_s \delta_s^2 \dot{\gamma}}, m, \phi, e_s \right) \quad (13)$$

Interpretation of Eq. (13) is facilitated by performing some simple algebraic manipulations to reframe three of the Π groups. First, $g/\delta_s \dot{\gamma}^2$ can be inverted to form a Savage number, $N_{sav} = \delta_s \dot{\gamma}^2/g$, which indicates whether grain interactions are likely to be dominated by inertial collisions or enduring gravitational contacts. Second, k/δ_s^2 can be combined with $\mu_f/\rho_s \delta_s^2 \dot{\gamma}$ to form a Darcy number, $N_{dar} = \mu_f/\rho_s k \dot{\gamma}$, which describes the tendency for restriction of pore-fluid flow to impede rearrangement of grains during shearing. Finally, $\mu_f/\rho_s \delta_s^2 \dot{\gamma}$ is a reciprocal Stokes number, which indicates the degree to which pore-fluid viscosity dampens grain inertia and consequent grain collisions (Raju and Meiburg, 1995). The Savage number, Darcy number and Stokes number have been used previously to categorize regimes of shear behavior in debris flows (Iverson, 1997), but this categorization is predicated on use of the Bagnold stress scaling noted above.

It is simple to rescale Eq. (13) to focus on the alternative regime in which enduring, gravitational grain contacts dominate stress generation. The rescaling can be accomplished by multiplying all parameters in Eq. (13) by $\rho_s \delta_s^2 \dot{\gamma}^2/\rho_s g H$ (except for the last three parameters, which are intrinsically dimensionless). The result is

$$\frac{\tau_{zx}}{\rho_s g H}, \frac{\tau_{zz}}{\rho_s g H} = f_9 \left(\frac{\langle v^2 \rangle^{1/2} \delta_s \dot{\gamma}}{g H}, \frac{\langle \omega^2 \rangle^{1/2} \delta_s \dot{\gamma}}{g H}, \frac{\delta_s \dot{\gamma}^2}{g}, \frac{k \dot{\gamma}^2}{g H}, \frac{\rho_f \delta_s^2 \dot{\gamma}^2}{\rho_s g H}, \frac{\delta_s}{H}, \frac{\mu_f \dot{\gamma}}{\rho_s g H}, m, \phi, e_s \right) \quad (14)$$

This expression includes the Savage number $N_{sav} = \delta_s \dot{\gamma}^2/g$ and the length-scale ratio δ_s/H that were identified in Eq. (13), reflecting the universal importance of these quantities.

Three new parameters on the right-hand side of Eq. (14) also deserve emphasis. First, the parameter $\rho_f \delta_s^2 \dot{\gamma}^2/\rho_s g H$ can be multiplied by the density ratio ρ_s/ρ_f to obtain the square of an inertia number defined as $N_I = \delta_s \dot{\gamma} / \sqrt{g H}$. A similar inertia number has been identified as a key parameter governing the effective rheology of dense granular flows that lack significant fluid effects (GDR MiDi, 2004; Forterre and

Pouliquen, 2008). The inertia number is closely related to the Savage number, but it additionally accounts for the effects of confining pressure that depends on the total flow thickness, H . Second, the parameter $\mu_f \dot{\gamma} / \rho_s gH$ in Eq. (14) is comparable to a viscous number N_v that has been identified as a key parameter governing the effective rheology of dense grain – fluid mixtures in which fluid viscosity is significant (Cassar et al., 2005; Boyer et al., 2011). The meaning of the third new parameter in Eq. (14), $k\dot{\gamma}^2/gH$, is relatively obscure, but its interpretation can be clarified by dividing it by $N_f^2 = \delta_s^2 \dot{\gamma}^2/gH$. This manipulation reduces $k\dot{\gamma}^2/gH$ to the simple ratio k/δ_s^2 , which appears in Eqs. (12) and (13) and reflects the influences of grain size and packing on permeability.

The scaling relationships summarized in Eqs. (12), (13) and (14) hold some clear implications for design of mesoscale experiments aimed at clarifying the effective rheology and mechanisms of stress generation in shearing grain – fluid mixtures. Equation (12), for example, demonstrates that a large number of dimensionless parameters might influence the behavior of geological mixtures involving diverse grains. Equations (13) and (14) show that better prospects exist for evaluating the behavior of idealized mixtures containing nearly identical spherical grains. The experiments of Boyer et al. (2011), for example, demonstrated that dense mixtures of liquid and uniform spheres exhibit Coulomb-like behavior (in which shear stress is proportional to effective normal stress) for a wide range of shear rates. However, these experiments also showed that the solid volume fraction m and Coulomb friction angle ϕ varied systematically as a function of the viscous number, $N_v = \mu_f \dot{\gamma} / \rho_s gH$. As N_v increased, m smoothly declined and ϕ smoothly increased, giving rise to a pseudo-viscous behavior regulated by normal stress. This behavior can be viewed as a form of Coulomb friction that is sensitive to rate- and state-dependent feedbacks (Iverson and George, 2014).

The existence of feedbacks that influence effective rheology indicates that the very notions of a prevalent landslide rheology or a debris-flow rheology may be flawed, because local material behavior may evolve in response to evolving large-scale dynamics (Iverson, 2003b; Iverson et al., 2010). Effects of such evolution are difficult to evaluate using dimensional analysis and are better addressed through formulation and normalization of differential equations that describe landslide and debris-flow dynamics.

4. Scaling inferred from differential equation normalization

Normalization of differential equations that describe the evolving dynamics of landslides and debris flows leads to scaling inferences that are more precise than those obtained from dimensional analysis. Similarly precise inferences result, for example, from normalization of the Navier-Stokes equations describing gravity-driven flow of a pure viscous fluid, which shows that the Reynolds and Froude numbers are the relevant scaling parameters for this phenomenon (Bird et al., 1960). However, scaling inferences obtained from differential equations are only as general – and as accurate – as the equations themselves.

Here I focus on scaling inferences obtained from a set of six differential equations that describe the depth-integrated dynamics of water-saturated landslides and debris flows that move across rigid, planar beds. The equations describe a system in which the thickness $h(x, y, t)$, the three vector components of the depth-integrated velocity, $\bar{u}(x, y, t)$, $\bar{v}(x, y, t)$, and $\bar{w}(x, y, t)$, the solid volume fraction, $m(x, y, t)$, and the basal pore-fluid pressure, $p_b(x, y, t)$, coevolve as functions of time, t , and the areal position coordinates, x and y (Fig. 3). Derivations, numerical solutions, and tests of the differential equations are presented elsewhere (George and Iverson, 2014; Iverson and George, 2014).

The choice of fundamental scales influences the outcome of equation normalization. Here, as in the dimensional analyses of Sections 3.1 and

3.2, I use scales appropriate for a debris flow or landslide with a characteristic length L and thickness H (Fig. 3). Because downslope motion of a landslide or debris flow is driven by gravitational potential, the scale is $(gL)^{1/2}$ for the x -velocity component \bar{u} and y -velocity component \bar{v} , whereas the scale for the z -direction velocity component \bar{w} is $(gH)^{1/2}$ (cf. Savage and Hutter, 1989). The scale $(gH)^{1/2}$ also applies for the depth-integrated debris dilation rate D , because $D \neq 0$ indicates that relative motion of solid and liquid phases occurs in the z direction (Iverson and George, 2014). The length scale L divided by the downslope velocity scale yields the time scale for downslope debris-flow motion, $(L/g)^{1/2}$. The scale for ρ is the initial static debris bulk density ρ_0 associated with the initial solid volume fraction m_0 : $\rho_0 = m_0 \rho_s + (1 - m_0) \rho_f$. The value m_0 also serves as the scale for m . Finally, the scale for all depth-averaged stress components ($\bar{\tau}_{xx}$, $\bar{\tau}_{yy}$, $\bar{\tau}_{zz}$, $\bar{\tau}_{yx}$, $\bar{\tau}_{zx}$, and $\bar{\tau}_{yz}$) and for the basal pore pressure p_b is $\rho_0 gH$. Use of these scales leads to definition of the following dimensionless quantities, denoted by asterisks:

$$\begin{aligned} x^* &= x/L, & y^* &= y/L, & z^* &= z/H, & t^* &= t/(L/g)^{1/2}, \\ u^* &= \bar{u}/(Lg)^{1/2}, & v^* &= \bar{v}/(Lg)^{1/2}, & w^* &= \bar{w}/(gH)^{1/2}, & h^* &= h/H, \\ D^* &= D/(gH)^{1/2}, & m^* &= m/m_0, & \rho^* &= \rho/\rho_0, & p^* &= p_b/\rho_0 gH, \\ (\bar{\tau}_{xx}^*, \bar{\tau}_{yy}^*, \bar{\tau}_{zz}^*, \bar{\tau}_{yx}^*, \bar{\tau}_{zx}^*, \bar{\tau}_{yz}^*) &= (\bar{\tau}_{xx}, \bar{\tau}_{yy}, \bar{\tau}_{zz}, \bar{\tau}_{yx}, \bar{\tau}_{zx}, \bar{\tau}_{yz})/\rho_0 gH \end{aligned} \tag{15}$$

Substitution of Eqs. (15) into the dimensional model equations derived by Iverson and George (2014) yields normalized forms of the equations. The normalized equations describing conservation of the x , y , and z components of momentum may be written as

$$\begin{aligned} \rho^* \left[\frac{\partial(h^* u^*)}{\partial t^*} + \frac{\partial(h^* u^{*2})}{\partial x^*} + \frac{\partial(hu^* v^*)}{\partial y^*} \right] - \varepsilon^{-1/2} \left(\rho^* - \frac{\rho_f}{\rho_0} \right) D^* u^* \\ = \rho^* h^* \frac{g_x}{g} + \varepsilon \left[\frac{\partial(\bar{\tau}_{yx}^* h^*)}{\partial y^*} - \frac{\partial(\bar{\tau}_{xx}^* h^*)}{\partial x^*} \right] - \tau_{zx}^*(0) \end{aligned} \tag{16}$$

$$\begin{aligned} \rho^* \left[\frac{\partial(h^* v^*)}{\partial t^*} + \frac{\partial(h^* v^{*2})}{\partial y^*} + \frac{\partial(hv^* u^*)}{\partial x^*} \right] - \varepsilon^{-1/2} \left(\rho^* - \frac{\rho_f}{\rho_0} \right) D^* v^* \\ = \rho^* h^* \frac{g_y}{g} + \varepsilon \left[\frac{\partial(\bar{\tau}_{xy}^* h^*)}{\partial x^*} - \frac{\partial(\bar{\tau}_{yy}^* h^*)}{\partial y^*} \right] - \tau_{zy}^*(0) \end{aligned} \tag{17}$$

and

$$\varepsilon^{1/2} \rho^* h^* \left[\frac{\partial w^*}{\partial t^*} + u^* \frac{\partial w^*}{\partial x^*} + v^* \frac{\partial w^*}{\partial y^*} \right] = \rho^* h^* \frac{g_z}{g} + \varepsilon \left[\frac{\partial(\bar{\tau}_{xz}^* h^*)}{\partial x^*} + \frac{\partial(\bar{\tau}_{yz}^* h^*)}{\partial y^*} \right] - \tau_{zz}^*(0) \tag{18}$$

where

$$\varepsilon = H/L \tag{19}$$

is a fundamental length-scale ratio that satisfies $\varepsilon \ll 1$ in most landslides and debris flows (cf., Savage and Hutter, 1989).

The normalized mass-conservation equations for the solid – fluid mixture and for the solid grains alone may be expressed as

$$\rho^* \left[\frac{\partial h^*}{\partial t^*} + \frac{\partial(h^* u^*)}{\partial x^*} + \frac{\partial(h^* v^*)}{\partial y^*} \right] = \varepsilon^{-1/2} \left(\rho^* - \frac{\rho_f}{\rho_0} \right) D^* \tag{20}$$

and

$$\rho^* \left[\frac{\partial(h^* m^*)}{\partial t^*} + \frac{\partial(h^* u^* m^*)}{\partial x^*} + \frac{\partial(h^* v^* m^*)}{\partial y^*} \right] = \varepsilon^{-1/2} \left(-\frac{\rho_f}{\rho_0} \right) D^* m^* \tag{21}$$

If these two equations are satisfied, then an analogous mass-conservation equation for the fluid phase is automatically satisfied (Iverson and George, 2014).

The normalized equation describing evolution of the basal pore-fluid pressure may be expressed as

$$\begin{aligned} \frac{\partial p^*}{\partial t^*} + u^* \frac{\partial p^*}{\partial x^*} + v^* \frac{\partial p^*}{\partial y^*} + \frac{(L/g)^{1/2}}{(\mu_f H^2/kE)} \frac{3}{h^{*2}} \left[p^* - \frac{\rho_f g_z}{\rho_0 g} h^* \right] \\ = \varepsilon^{-1/2} \frac{D^*}{4\rho^*} \frac{\rho_f g_z}{\rho_0 g} \left(\rho^* - \frac{\rho_f}{\rho_0} \right) - \left[\frac{g_z h^*}{g} \frac{\partial u^*}{\partial x^*} + \frac{\partial v^*}{\partial y^*} \right] \left(3\rho^* + \frac{\rho_f}{\rho_0} \right) \quad (22) \\ - \varepsilon^{-1} \frac{E}{\rho_0 g H} \frac{3\sqrt{u^{*2} + v^{*2}}}{h^*} \left[m_0 m^* - \frac{m_{crit}}{1 + \sqrt{N}} \right] \end{aligned}$$

where m_{crit} is a static, critical-state value of m (i.e., the equilibrium value of m following large deformations), and N is a dimensionless state parameter defined as $N = \mu_f \dot{\gamma} / [\rho_s \dot{\gamma}^2 \delta_s^2 + \rho g_z h - p_b]$. This definition shows that N is a generalized version of the viscous number N_V described in section 3.3 (Iverson and George, 2014).

Finally, the model includes a closure equation that employs Darcy's law and mass conservation to relate the depth-averaged dilation rate $D(x, y, t)$ to the basal pore-fluid pressure. The normalized version of this closure equation is

$$D^* = \varepsilon^{1/2} \frac{\rho_0 g H}{E} \left(\frac{(L/g)^{1/2}}{(\mu_f H^2/kE)} \right) \left[p^* - \frac{\rho_f g_z}{\rho_0 g} h^* \right] \quad (23)$$

Mathematically, the set of normalized model equations (Eqs. 16 through 23) is rather complicated, but the equations contain relatively few dimensionless parameters. Values of these parameters, in addition to initial conditions, dictate the behavior of solutions (George and Iverson, 2014). Three of the parameters, g_x/g , g_y/g , and g_z/g , reflect the extrinsic influence of the local slope angle θ and orientation, which are independent of the properties of a landslide or debris flow. The remaining eight parameters express the influence of landslide or debris-flow geometry or material properties:

$$\varepsilon, \quad m_{crit}, \quad \frac{\rho_f}{\rho_0}, \quad \frac{(L/g)^{1/2}}{\mu_f H^2/kE}, \quad \frac{\rho_0 g H}{E}, \quad \phi, \quad \frac{\rho_0 H(gL)^{1/2}}{\mu_f}, \quad \frac{\rho_0 g H}{c_f} \quad (24)$$

The first five of these parameters appear explicitly in Eqs. (16) through (23), whereas the last three parameters are contained implicitly in Eqs. (16) and (17) as a result of boundary shear tractions $\tau_{zx}(0)$ and $\tau_{zy}(0)$ that depend on the granular Coulomb friction angle, ϕ , and on the cohesion c_f and viscosity μ_f of pore fluid that may contain suspended mud particles. Importantly, each of the dimensionless parameters listed in Eq. (24) – or closely related surrogates for these parameters – also appears in Eq. (9), which was obtained by different means. Only a few quantities in Eq. (9) do not appear in Eq. (24), and these quantities are either embedded implicitly in the definitions provided in Eq. (15), or they are superfluous in the present context (i.e., in a landslide or debris flow that is saturated with water). The agreement of the results in Eq. (9) and Eq. (24) illustrates the fact that dimensional analysis and differential equation normalization provide synergistic tools for inferring scaling relationships.

From the standpoint of experiment design, Eq. (9) and Eq. (24) yield the same key inference: downsizing from prototype scale to experiment scale is complicated by the fact that the scaling parameter $(L/g)^{1/2}/(\mu_f H^2/kE)$ decreases in proportion to H^2 , whereas the parameter $\rho_0 H(gL)^{1/2}/\mu_f$ increases in proportion to H , and each parameter contains the pore-fluid viscosity μ_f in its denominator. As detailed in section 3.2, these trends point to an inevitable tendency for miniaturized laboratory landslides to exhibit disproportionately small effects of pore-pressure evolution

and disproportionately large effects of pore-fluid shear resistance. Therefore, in small-scale experiments, any excess pore-fluid pressure generated by landslide or debris-flow motion will dissipate too rapidly to mimic behavior in full-scale prototypes.

Differential equation normalization yields additional insight that cannot be obtained from dimensional analysis. The normalization described above demonstrates the role of the length-scale ratio $\varepsilon = H/L$, which appears in Eqs. (16) through (23). Because $\varepsilon \ll 1$ applies in many landslides and debris flows (Fig. 3), terms containing the factor ε or $\varepsilon^{1/2}$ in Eqs. (16) through (23) are generally small in comparison to other terms. On the other hand, the term in Eq. (22) containing ε^{-1} is the single most important term in the model. It demonstrates the over-arching importance of pore-pressure evolution coupled to changes in m . Such inferences regarding the probable magnitudes of various physical effects are useful for targeting objectives in experiments and also for guiding numerical computations. In some cases the high-order terms containing ε or $\varepsilon^{1/2}$ in Eqs. (16)–(23) may be entirely negligible.

5. Initial and boundary conditions

The foregoing results emphasize criteria for evaluating the dynamic similarity of water-laden landslides and debris flows at laboratory and field scales. These criteria are crucial for guiding experiment design, but they are not the only important considerations. Other key concerns involve the effects of initial and boundary conditions.

Effects of initial conditions can be evaluated in a simple way by comparing the initial geometries and force balances of geomorphic prototypes and laboratory models. Most natural landslides and debris flows evolve from static masses of material that are poised in states of mechanical equilibrium on slopes. Movement generally begins in response to a small perturbation of this balanced initial state (George and Iverson, 2014). Such perturbations may result from gradual changes in pore-water pressure or gradual erosion of the toe of a slope, for example. By contrast, many laboratory mass-movement experiments use dam-break initial conditions, in which granular debris is retained behind a gate and then suddenly released (e.g., Iverson et al., 2010; Mangeney et al., 2010). This dam-break type of initial condition is both convenient and replicable, but it violates geometric similarity with most geomorphic prototypes. Moreover, in dam-break experiments a large force imbalance develops almost instantaneously as a free face of debris is exposed during opening of the headgate, and the flow front is driven rapidly downslope by this force imbalance (e.g., Figs. 4 and 6). Thus, although dam-break experiments with either wet or dry debris can have great value for testing mathematical models, they cannot be used as scale models of geomorphic prototypes. This problem is most severe if the height of the dam face is large enough to be comparable to the total height descended by an experimental landslide or debris flow.

A different type of shortcoming exists in dynamic steady-state experiments, which are commonly used to investigate debris-flow rheology (e.g., Parsons et al., 2001). Imposing an initial steady state excludes the physical effects summarized in the key dimensionless time scale ratio $(L/g)^{1/2}/(\mu_f H^2/kE)$ identified in Eqs. (9) and (24). In such experiments, any tendency for the state of deforming grain-fluid mixtures to evolve is removed *a priori*. Thus, although steady-state rheology experiments are important in many contexts, they may lack the necessary degrees of freedom to reveal crucial features of landslide and debris-flow dynamics (Iverson, 2003b).

Boundary conditions also play a critical role in designing experiments intended to improve understanding of landslides and debris flows. Most experiments performed to date have involved motion across rigid beds (e.g., Iverson et al., 2004, 2010; Pudasaini and Hutter, 2007). By contrast, many natural landslides and debris flows travel across deformable, erodible beds, and interactions with such beds can produce profound feedbacks, particularly if the bed sediment is wet (Fig. 9). Scaling considerations that apply to a moving tabular mass also apply to a layer of static sediment that exchanges momentum



Fig. 9. Photograph of an experimental debris flow growing dramatically in mass and momentum as it interacts with a wet, erodible sediment bed in the USGS debris-flow flume on 19 September 2006. The highly agitated flow front advancing beneath the flume-spanning crossbeam carries some light-colored blocks of foam that were used to seal the flume headgate prior to release of the debris flow (see Iverson et al., 2011). Video recordings of this experiment and many similar experiments are viewable at <http://pubs.usgs.gov/of/2007/1315/> (see Logan and Iverson, 2007).

with that mass during erosion or deposition by a landslide or debris flow (Iverson, 2012; Iverson and Ouyang, 2015). This scaling, along with experimental data, indicates that pressurization of pore water in overridden basal sediment may be a very effective mechanism for reducing basal friction and enhancing landslide and debris-flow runout, provided that the sediment bed and the overriding mass are thick enough (Iverson et al., 2011). This type of scale-dependent friction reduction points to a simple explanation for the surprisingly long runouts of many large landslides (Iverson, 1997; Legros, 2002).

6. Concluding discussion: design and relevance of geomorphological experiments

Experimental investigations of landslides and debris flows have direct geomorphological relevance only if they employ appropriate scaling and initial and boundary conditions. Many experiments and analyses performed over the past few decades to investigate granular flows and grain – fluid physics have limited relevance for understanding and interpreting the behavior of landslides and debris flows – because the scale, initial conditions, or boundary conditions are inappropriate. Indeed, designers of landslide and debris-flow experiments must confront scaling problems that designers of granular physics experiments can commonly disregard.

One key difference between landslide and debris-flow experiments and many granular physics experiments arises from the differing characters of the grains themselves. The goal of physics experiments is generally to distil a phenomenon to its simplest possible form. For that reason, such experiments commonly employ grains consisting of identical rigid spheres. By contrast, grains in landslides and debris flows

typically consist of irregular rock fragments with sizes that span many orders of magnitude. An assemblage of incompressible spheres in contact with one another has no elastic component of compressibility because any volume change must be accommodated by irreversible slip at grain contacts. By contrast, an assemblage of irregular, incompressible grains can exhibit a finite bulk elastic compressibility ($1/E$) because some porosity change can be accommodated by elastic shear distortions of angular grain contacts. Thus, the presence of E in the crucial timescale ratio $(L/g)^{1/2}/(\mu_f H^2/kE)$ identified in the foregoing sections of this paper provides evidence that evolving, gravity-driven flows of natural sediment mixtures may exhibit behaviors that differ fundamentally from those involving mixtures of uniform, incompressible spheres.

Other difficulties in designing relevant landslide and debris-flow experiments arise as a result of the physical properties of the pore fluid. Sediment mixtures commonly undergo significant porosity changes as they are loaded or as they shear, and these porosity changes produce pore-pressure changes that are proportional to the pore-fluid viscosity, μ_f . The effect of pore-fluid viscosity on pore pressure (and hence on frictional resistance to motion) increases with landslide or debris-flow size, as indicated by the factor $\mu_f H^2$ in $(L/g)^{1/2}/(\mu_f H^2/kE)$. On the other hand, the effect of pore-fluid viscosity and cohesive yield strength on mass-movement resistance decreases with landslide or debris-flow size. Miniaturized experiments consequently exhibit pore-fluid pressure effects that are too small and pore-fluid shear resistance effects that are too large, relative to those exhibited in large-scale field phenomena. An exacerbating factor is that natural mixtures of irregular grains have hydraulic permeabilities (k values) that are smaller than those of assemblages of identical spheres because small grains impede the flow of fluid between larger grains. The low k values of natural sediments increase solid-fluid drag and the potential for development of persistent high pore-fluid pressures in gravity-driven flows of grain-fluid mixtures.

The scaling considerations summarized here imply that, although experimentation can contribute greatly to understanding of landslides and debris flows, experiments must be designed with care, and experimental results must be interpreted with a healthy dose of skepticism. In particular, the geomorphological insight gained from experiments cannot be judged on the basis of superficial morphometric similarities of experimental and natural landforms. Consider a miniature debris-flow fan built by flows involving $< 1 \text{ m}^3$ of muddy sand in a laboratory. Although the laboratory fan may superficially resemble a natural debris-flow fan built by gravel- and boulder-rich flows that are 10^6 times larger, motion of the flows that formed the laboratory fan may be resisted largely by fluid viscosity, cohesion, and surface tension, whereas motion of field-scale debris flows is resisted largely by Coulomb friction regulated by evolving pore-fluid pressure (Iverson, 2003b). Thus, in landslide and debris-flow experiments – and perhaps in many other geomorphological experiments – similarity of form does not imply similarity of process. Scaling analyses of experiment dynamics therefore add perspective that cannot be attained by inspection of experiment outcomes alone.

References

- Armanini, A., Fraccarollo, L., Capart, H., Larcher, M., 2005. Rheological stratification in experimental free-surface flows of granular-liquid mixtures. *J. Fluid Mech.* 532, 269–319. <http://dx.doi.org/10.1017/S0022112005004283>.
- Bagnold, R.A., 1954. Experiments on a gravity-free dispersion of large solid spheres in a Newtonian fluid under shear. *Proc. R. Soc. London, Ser. A* 225, 49–63.
- Baker, V.R., 1996. Hypotheses and geomorphological reasoning. In: Rhoads, B.L., Thorn, C.E. (Eds.), *The scientific nature of geomorphology*. Wiley, New York, pp. 57–85.
- Bird, R.B., Stewart, W.E., Lightfoot, E.N., 1960. *Transport phenomena*. Wiley, New York.
- Bolster, D., Hershberger, R.E., Donnelly, R.J., 2011. Dynamic similarity, the dimensionless science. *Phys. Today* 64, 42–47.
- Bowman, E.T., Take, W.A., Rait, K.L., Haan, C., 2012. Physical models of rock avalanche spreading behaviour with dynamic fragmentation. *Can. Geotech. J.* 49, 460–476.
- Boyer, F., Guazzellu, E., Pouliquen, O., 2011. Unifying suspension and granular rheology. *Phys. Rev. Lett.* 107, 188301.
- Bridgman, P., 1922. *Dimensional analysis*. Yale University Press, New Haven (112 pp.).
- Buckingham, E., 1914. On physically similar systems; illustrations of the use of dimensional equations. *Phys. Rev.* 4, 345–376.

- Buckingham, E., 1915. Model experiments and the forms of empirical equations. *Trans. Am. Soc. Mech. Eng.* 37, 263–296.
- Bugnion, L., McArdell, B.W., Bartelt, P., Wendeler, C., 2012. Measurements of hillslope debris flow impact pressure on obstacles. *Landslides* 9, 179–187. <http://dx.doi.org/10.1007/s10346-011-0294-4>.
- Cassar, C., Nicolas, M., Pouliquen, O., 2005. Submarine granular flows down inclined planes. *Phys. Fluids* 17, 103301.
- Dade, W.B., Huppert, H.H., 1998. Long runout rockfalls. *Geology* 26, 803–806.
- Deboeuf, A., Gauthier, G., Martin, J., Yorkovetsky, Y., Morris, J.F., 2009. Particle pressure in a sheared suspension: a bridge from osmosis to granular dilatancy. *Phys. Rev. Lett.* 102, 108031. <http://dx.doi.org/10.1103/PhysRevLett.102.108031>.
- Densmore, A.L., Anderson, R.S., McAadoo, B.G., Ellis, M.A., 1997. Hillslope evolution by bed-rock landslides. *Science* 275, 369–372.
- Eckersley, D., 1990. Instrumented laboratory flowslides. *Geotechnique* 40, 489–502.
- Forterre, Y., Pouliquen, O., 2008. Flows of dense granular media. *Annu. Rev. Fluid Mech.* 40, 1–24.
- George, D.L., Iverson, R.M., 2014. A depth-averaged debris-flow model that includes the effects of evolving dilatancy: 2. numerical predictions and experimental tests. *Proc. R. Soc. London, Ser. A* 470 <http://dx.doi.org/10.1098/rspa.2013.0820>.
- Gilbert, G.K., 1914. The transportation of debris by running water. U.S. Geological Survey Professional Paper 86. U.S. Government Printing Office, Washington, D.C.
- Goldhirsch, I., 2003. Rapid granular flows. *Annu. Rev. Fluid Mech.* 35, 267–293.
- Heim, A., 1882. Der bergsturz von Elm. *Z. Dtsch. Geol. Ges.* 34, 74–115.
- Hsü, K.J., 1978. Albert Heim: observations on landslides and relevance to modern interpretations. In: Voight, B. (Ed.), *Rockslides and avalanches*, 1, natural phenomena. Elsevier, Amsterdam, pp. 71–93.
- Hsu, L., Dietrich, W.E., Sklar, L.S., 2014. Mean and fluctuating basal forces generated by granular flows: Laboratory observations in a large vertically rotating drum. *J. Geophys. Res. Earth Surf.* 119 <http://dx.doi.org/10.1002/2013JF003078>.
- Hunt, M.L., Zenit, R., Campbell, C.S., Brennen, C.E., 2002. Revisiting the 1954 suspension experiments of R.A. Bagnold. *J. Fluid Mech.* 452, 1–24.
- Iverson, R.M., 1997. The physics of debris flows. *Rev. Geophys.* 35, 245–296.
- Iverson, R.M., 2003a. How should mathematical models of geomorphic processes be judged? In: Wilcock, P.R., Iverson, R.M. (Eds.), *Prediction in Geomorphology*, Geophys. Monograph 135. American Geophysical Union, Washington, D.C., pp. 83–94.
- Iverson, R.M., 2003b. The debris-flow rheology myth. In: Rickenmann, D., Chen, C.L. (Eds.), *Debris-flow Hazards Mitigation: Mechanics, Prediction, and Assessment v. 1*. Millpress, Rotterdam, pp. 303–314.
- Iverson, R.M., 2005. Regulation of landslide motion by dilatancy and pore pressure feedback. *J. Geophys. Res.* 110, (F02015). <http://dx.doi.org/10.1029/2004JF000268>.
- Iverson, R.M., 2012. Elementary theory of bed-sediment entrainment by debris flows and avalanches. *J. Geophys. Res.* 117, (F03006). <http://dx.doi.org/10.1029/2011JF002189>.
- Iverson, R.M., Denlinger, R.P., 2001. Flow of variably fluidized granular masses across three-dimensional terrain: 1. Coulomb mixture theory. *J. Geophys. Res.* 106, 537–552.
- Iverson, R.M., George, D.L., 2014. A depth-averaged debris-flow model that includes the effects of evolving dilatancy: 1. physical basis. *Proc. R. Soc. London, Ser. A* 470 <http://dx.doi.org/10.1098/rspa.2013.0819>.
- Iverson, R.M., LaHusen, R.G., 1989. Dynamic pore-pressure fluctuations in rapidly shearing granular materials. *Science* 246, 796–799.
- Iverson, R.M., Ouyang, C., 2015. Entrainment of bed material by Earth-surface mass flows: review and reformulation of depth-integrated theory. *Rev. Geophys.* 53. <http://dx.doi.org/10.1002/2013RG000447>.
- Iverson, R.M., Reid, M.E., LaHusen, R.G., 1997. Debris-flow mobilization from landslides. *Annu. Rev. Earth Planet. Sci.* 25, 85–138.
- Iverson, R.M., Reid, M.E., Iverson, N.R., LaHusen, R.G., Logan, M., Mann, J.E., Brien, D.L., 2000. Acute sensitivity of landslide rates to initial soil porosity. *Science* 290, 513–516.
- Iverson, R.M., Logan, M., Denlinger, R.P., 2004. Granular avalanches across irregular three-dimensional terrain: 2. experimental tests. *J. Geophys. Res.* 109, F01015. <http://dx.doi.org/10.1029/2003JF000084>.
- Iverson, R.M., Logan, M., LaHusen, R.G., Berti, M., 2010. The perfect debris flow: aggregated results from 28 large-scale experiments. *J. Geophys. Res.* 115, F03005. <http://dx.doi.org/10.1029/2009JF001514>.
- Iverson, R.M., Reid, M.E., Logan, M., LaHusen, R.G., Godt, J.W., Griswold, J.G., 2011. Positive feedback and momentum growth during debris-flow entrainment of wet bed sediment. *Nat. Geosci.* 4, 116–121. <http://dx.doi.org/10.1038/NGEO1040>.
- Kaitna, R., Dietrich, W.E., Hsu, L., 2014. Surface slopes, velocity profiles and fluid pressure in coarse-grained debris flows saturated with water and mud. *J. Fluid Mech.* 741, 377–403. <http://dx.doi.org/10.1017/jfm.2013.675>.
- Legros, F., 2002. The mobility of long-runout landslides. *Eng. Geol.* 63, 301–331.
- Logan, M., Iverson, R.M., 2007. Video documentation of experiments at the USGS debris-flow flume 1992–2006 (amended to include 2007–2013). U.S. Geological Survey Open-file report 2007–1315 v. 1.3 (<http://pubs.usgs.gov/of/2007/1315/>).
- Mangeney, A., Roche, O., Hungr, O., Mangold, N., Faccanoni, G., Lucas, A., 2010. Erosion and mobility in granular collapse over sloping beds. *J. Geophys. Res.* 115, F03040. <http://dx.doi.org/10.1029/2009JF001462>.
- Manzella, I., Labiouse, V., 2009. Flow experiments with gravel and blocks at small scale to investigate parameters and mechanisms involved in rock avalanches. *Eng. Geol.* 109, 146–158.
- MiDi, G.D.R., 2004. On dense granular flows. *Eur. Phys. J. E* 14, 341–365.
- Montgomery, D.R., Dietrich, W.E., Torres, R., Anderson, S.P., Heffner, J.T., Loague, K., 1997. Piezometric response of a steep unchanneled valley to natural and applied rainfall. *Water Resour. Res.* 33, 91–109. <http://dx.doi.org/10.1029/96WR02985>.
- Montgomery, D.R., Schmidt, K.M., Dietrich, W.E., McKean, J., 2009. Instrumental record of debris flow initiation during natural rainfall: Implications for modeling slope stability. *J. Geophys. Res.* 114, F01031. <http://dx.doi.org/10.1029/2008JF001078>.
- Moriwaki, H., Inokuchi, T., Hattajji, T., Sassa, K., Ochiai, H., Wang, G., 2004. Failure processes in a full-scale landslide experiment using a rainfall simulator. *Landslides* 1, 277–288.
- Ochiai, H., Okada, Y., Furuya, G., Okura, Y., Matsui, T., Sammori, T., Terajima, T., Sassa, K., 2004. A fluidized landslide on a natural slope by artificial rainfall. *Landslides* 1, 211–219.
- Ochiai, H., Sammori, T., Okada, Y., 2007. Landslide experiments on artificial and natural slopes. In: Sassa, K., Fukuoka, H., Wang, F., Wang, G. (Eds.), *Progress in landslide science*. Springer, Berlin, pp. 209–226.
- Okura, Y., Kitahara, H., Sammori, T., Kamanawi, A., 2000. The effects of rockfall volume on runout distance. *Eng. Geol.* 109–124.
- Paguican, E.M.R., van Wyk de Vries, B., Lagmay, A., 2014. Hummocks: how they form and how they evolve in rockslide-debris avalanches. *Landslides* 11, 67–80.
- Paik, J., Son, S., Kim, T., Kim, S., 2012. Real scale field experiment of debris flow for investigating its deposition and entrainment. Video presentation at 2012 Fall Meeting of the American Geophysical Union, San Francisco.
- Parsons, J.D., Whipple, K.X., Simoni, A., 2001. Experimental study of the grain-flow, fluid-mud transition in debris flows. *J. Geol.* 109, 427–447.
- Pudasaini, S., Hutter, K., 2007. *Avalanche dynamics*. Springer, Berlin.
- Raju, N., Meiburg, E., 1995. The accumulation and dispersion of heavy particles in forced two-dimensional mixing layers. Part 2: the effect of gravity. *Phys. Fluids* 7, 1241–1264.
- Reid, M.E., LaHusen, R.G., Iverson, R.M., 1997. Debris-flow initiation experiments with diverse hydrologic triggers. In: Chen, C.L. (Ed.), *Debris-flow hazards mitigation: mechanics, prediction, and assessment*. American Soc. of Civil Engineers, New York, pp. 1–11.
- Rice, J.R., Cleary, M.P., 1976. Some basic stress diffusion solutions for fluid-saturated elastic porous media with compressible constituents. *Rev. Geophys.* 14, 227–241.
- Rickenmann, D., Weber, D., Stepanov, B., 2003. Erosion by debris flows in field and laboratory experiments. In: Rickenmann, D., Chen, C.-I. (Eds.), *Debris-flow Hazards Mitigation: Mechanics, Prediction, and Assessment v. 2*. Millpress, Rotterdam, pp. 883–894.
- Roche, O., Montserrat, S., Niño, Y., Tamburrino, A., 2010. Pore fluid pressure and internal kinematics of gravitational laboratory air-particle flows: Insights into the emplacement dynamics of pyroclastic flows. *J. Geophys. Res.* 115, B09206. <http://dx.doi.org/10.1029/2009JB007133>.
- Savage, S.B., 1984. The mechanics of rapid granular flows. *Adv. Appl. Mech.* 24, 289–366.
- Savage, S.B., Hutter, K., 1989. The motion of a finite mass of granular material down a rough incline. *J. Fluid Mech.* 199, 177–215.
- Schaeffer, D.G., Iverson, R.M., 2008. Steady and intermittent slipping in a model of landslide motion regulated by pore-pressure feedback. *SIAM J. Appl. Math.* 69, 769–786.
- Shreve, R.L., 1968. The Blackhawk landslide. *Geol. Soc. Am. Spec. Pap.* 108.
- Springman, S.M., Kienzler, P., Casini, F., Askarinejad, A., 2009. Landslide triggering experiment in a steep forested slope in Switzerland. In: Hamza, M., et al. (Eds.), 17th International Conference on Soil Mechanics & Geotechnical Engineering. IOS Press, pp. 1698–1701 <http://dx.doi.org/10.3233/978-1-60750-031-5-1698>.